Journal of Solid Waste Valorization and Chemical Management, 2026, Vol. 01

ARTICLE DOI: 10.66729/jswvcm202604003

Numerical Simulation Study on Meso-structure Fracture of Waste Rock Tailings Cemented Backfill with Different Initial Defects

Kang Zhao[1,2,*], Daotan Wen[2], Weiling Xiao[2], Yajing Yan[1], Juncheng Zhong[2]

1 Solids Waste and Chemicals Management Center, Ministry of Ecology and Environment, Beijing 100029, China.
2 School of Civil and Surveying & Mapping Engineering, Jiangxi University of Science and Technology, Ganzhou Jiangxi 341000, China.

*Corresponding Author: Kang Zhao; E-mail: zkky2021@163.com

Abstract

Utilizing tailings as aggregate and cementitious material to backfill underground mined-out areas not only ensures mining safety but also enables large-scale disposal of tailings solid waste. A thorough understanding of the effect of initial defects on the mechanical properties of cemented backfill can help optimize design while improving engineering safety and stability. This study employed the finite element software ABAQUS to numerically simulate the microstructural evolution of backfill materials. First, a model generation algorithm was used to construct two-dimensional meso-numerical models of cemented bodies with varying porosity. A convergence study on mesh size was conducted using pre-inserted cohesive elements. Subsequently, displacement loading was applied to analyze the complete process from crack initiation to propagation in the numerical models. Finally, an in-depth investigation of the stress-strain curves was performed. The results demonstrate that: (1) with increasing porosity, both the number of fractured elements and the total crack length in backfill models under uniaxial compression gradually decrease; (2) when porosity increases from 0% to 1.5%, the compressive strength decreases by 18.6%; (3) although porosity influences crack initiation in backfill specimens, their ultimate failure processes remain similar. The numerical model was validated against experimental data from the literature, showing good agreement in both peak strength and stress-strain behavior. This provides fundamental support for understanding the stability of tailings-cemented backfill systems and offers a reference for more complex meso-numerical studies of cemented backfill materials.

Keywords

Waste rock-tailings cemented body; Initial defects; Stress-strain; Mesoscopic model; Porosity; Crack characteristics

Citation: Kang Zhao, Daotan Wen, Weiling Xiao and *et al*. Numerical Simulation Study on Meso-structure Fracture of Waste Rock Tailings Cemented Backfill with Different Initial Defects. *Journal of Solid Waste Valorization and Chemical Management.* 2026, 01 (1): 1-12. doi: 10.66729/jswvcm202604003.

Highlights

- Waste tailings cemented filler is seen as a four-phase composite.
- Porosity's significant impact on material mechanics is highlighted.
- Simulation of microscopic damage evolution process.
- The results are compared with the experimental results in the literature.

1.Introduction

With economic growth, the efficient development of non-renewable metals has become a key aspect of green mining for mining enterprises[1]. Mining is the backbone of national development. As shallow resources are exhausted, most mines are turning to deep mining[2,3], facing challenges such as high risk, high cost, and low efficiency[4-6], which generate large amounts of mine solid waste and goaf cavities[7,8]. As the main supporting structure of the goaf, the material and mechanical properties of cemented backfill are very important for ensuring goaf safety. As a filling material, tailings can not only effectively support the movement of overlying rock in underground goafs but also reduce the land occupation of tailings storage and associated environmental pollution[9-11]. As mining gradually enters deep extraction, dry filling can no longer meet the requirements of green mining. Waste rock and tailings consolidated backfill is a heterogeneous brittle material composed of waste rock aggregate, tailings, and cementitious material, and it contains initial defects such as pores and micro-cracks[12-16]. Micromechanics research shows that damage accumulation and development in the microstructure of heterogeneous brittle composites are the direct causes of their macroscopic failure[17-19].

Numerical methods have been widely adopted to link the microstructure of composite materials to their macroscopic mechanical behavior[20-22]. In this context, ABAQUS (Dassault Systèmes SIMULIA Corp., Rhode Island, RI, USA) and PFC (Itasca Consulting Group, Inc., Minneapolis, Minnesota, MN, USA) have become standard platforms. For example, Abera[23] employed ABAQUS to simulate variable-stiffness composite shells. Huang[24] used PFC2D to examine the evolution of pores and cracks in coal gangue cemented fill. Xu[25] developed a rate-dependent cohesive model within ABAQUS for the dynamic fracture of two-phase materials. In the specific field of cemented backfill, Xin[26] developed a two-dimensional meso-scale model focusing on the effect of waste

Copyright:© 2026 The Author(s). Published by ICJN Press.
This is an open access article under the https://creativecommons.org/licenses/by/4.0/
Received 1 April 2026; Revised 27 April 2026; Accepted 25 May 2026; Available online 28 May 2026.

rock content. Wang[27] investigated the fracture behavior of the interfacial transition zone (ITZ) under different stress angles. Shi[28] identified three distinct damage modes in backfill composites using particle flow simulations. Collectively, these studies confirm that numerical simulation is an effective tool for relating microstructure to mechanical performance in backfill materials.

Despite these advances, two significant gaps remain. First, existing meso-scale models of cemented backfill predominantly treat the material as a two- or three-phase composite, with pores either neglected or implicitly smeared into the matrix properties. Yet waste rock-tailings cemented backfill inherently contains a large number of meso-scale pores[29]. These pores critically influence crack initiation and propagation. Explicit four-phase modelling — in which pores are geometrically represented as a distinct phase alongside aggregates, mortar, and the ITZ — remains scarce. This is an important gap because explicit pore representation allows cracks to nucleate directly from pore boundaries, a mechanism that cannot be captured by continuum approaches. Second, systematic studies that isolate the effect of porosity by comparing porous and non-porous specimens under otherwise identical conditions are lacking. Most existing investigations vary porosity indirectly through changes in mix design, making it difficult to decouple the effect of pores from that of other factors.

To address these gaps, the present study models waste rock-tailings cemented backfill as an explicit four-phase composite comprising waste rock aggregates, mortar matrix, ITZ, and pores. By generating multiple stochastic specimens with identical aggregate configurations but different porosity levels (0% to 1.5%), this work isolates the effect of porosity on crack initiation, propagation, and macroscopic strength. Furthermore, the numerical model is quantitatively validated against published experimental data before parametric analyses are conducted.

The aim of this study is to numerically analyze the mechanical behavior of a fine-scale model of waste rock-tailings cemented backfill, considering initial defects. Based on reported experimental results and numerical analyses, the input material parameters are set to establish a fine-scale model of waste rock-tailings cemented backfill with different porosities. The effects of porosity on the crack initiation and propagation mechanism, crack characterization, and stress-strain relationship under compression are discussed in depth, as well as the effects of porosity on the compressive properties of the backfill members. This work explicitly represents pores as a distinct geometric phase. It compares porous and non-porous specimens under identical aggregate configurations to isolate the effects of porosity. It also characterizes damage through three complementary indicators: ruptured elements, crack length, and stress-strain response. This provides mechanistic insights that cannot be obtained from macroscopic experiments alone.

2.Mesoscopic Model of Filling Body

Generally speaking, the meso-structure of cemented backfill is composed of coarse and fine aggregates, pores, mortar, and the ITZ. Coarse aggregates have various shapes, such as gravel and pebbles. Because random polygonal aggregates require higher computational power and longer computation time, this study assumes that the coarse aggregates are simplified to circular shapes and the pores are likewise simplified to circular shapes. The ITZ is a relatively critical factor and is typically embedded between the aggregate and the mortar matrix.

2.1 Size Distribution of Aggregates and Pores

The coarse aggregate gradation of the backfill, as determined by Talbot grading theory, has been shown to yield good structural density and strength. According to the theoretical grading formula, the particle content of each size can be determined, enabling the proportion of each aggregate to be calculated. The Talbot grading formula can be expressed as follows:

$$P = 100\left(\frac{d}{D}\right)^n \quad (1)$$

Where P is the percentage passing for each particle size (%); d is the particle size of the aggregate (mm); D is the maximum aggregate particle size (mm), and n is the Talbot size grading index, generally taken between 0.3 and 0.7.

In this study, waste rock and tailings are selected as filling aggregate, and composite Portland cement is used as the cementitious material to mix tailings and waste rock for backfilling, which can overcome the defects of waste rock segregation and stratification. For simplicity, only coarse aggregates larger than 1 mm are modeled. It is assumed that the pores are circular with a size range of 1 mm – 2 mm. A large number of small fine aggregates are considered part of the mortar together with the cement matrix, assuming their mechanical properties are uniform. The pore area fraction is expressed as the porosity. In this paper, the diameter ranges of the coarse aggregate are 1 mm – 2 mm, 2 mm – 4 mm, 4 mm – 6 mm, 6 mm – 8 mm, 8 mm – 10 mm, and 10 mm – 12 mm. According to existing studies, a grading index higher than 0.5 with tailings mixed in proportion as filling aggregate yields a better filling effect[30]. Therefore, a two-dimensional numerical model of cemented backfill with a length of 50 mm, a height of 100 mm, a waste rock content of 50%, and a grading index n of 0.6 was established. From equation (1), the content of coarse aggregate of each grain size can be calculated, by which the distribution of aggregate particles with Talbol grading index n of 0.6 was obtained, as shown in **Table 1**.

Table 1. Aggregate Particle Distribution of Talbol Gradation Indices

n	Particle volume fraction at different size intervals (mm)（%）					
	1 - 2	2 - 4	4 - 6	6 - 8	8 - 10	10 - 12
0.6	34.12	17.60	14.24	12.42	11.24	10.36

2.2 Aggregate and Pore Generation

The establishment and analysis of composite mesoscopic models is now well established, with a large body of literature available[31,32]. There are various forms of aggregates, such as two-dimensional (round, oval, random polygon) and three-dimensional (spherical, oval, random convex polygon). Two main types of finite element models exist: mesh-mapping aggregate models and geometric-boundary aggregate models[33]. The two modeling approaches have different emphases. Mesh mapping defines material properties on an existing mesh without modifying the model, resulting in a more orderly configuration. By contrast, the geometric-boundary approach can accurately describe aggregate shapes, and interface characteristics can be simulated using cohesive elements embedded along the boundaries.

The geometric-boundary aggregate model adopted in this paper repeatedly generates and places aggregates and pores until the target area is completely filled. The shapes of aggregates and pores are simplified to circles. The formation and accumulation process of backfill aggregate at the mesoscale is shown in **Figure. 1**. The

meso-geometric shape is obtained by controlling the sample size, coarse aggregate volume fraction, porosity and pore size range, coarse aggregate particle size range, and aggregate gradation. The specific steps are as follows:

(1) Input control parameters: specimen size, coarse aggregate volume fraction, porosity, aggregate gradation, pore size range.

(2) Generate random coarse aggregates and pores based on size range and shape constraints.

(3) Randomly place aggregates and pores into a predetermined area subject to physical constraints. Check for overlap or intersection. If overlap occurs, return to step 2; otherwise, proceed to the next step.

(4) Determine the total fraction of aggregate and pore space. If the target value is not reached, return to step 2; otherwise, end the process.

It should be noted that waste rock aggregates in practice often exhibit angular or irregular shapes due to crushing, whereas this study idealizes them as circular for the following reasons. First, the focus of this work is the influence of initial pores (porosity) rather than aggregate morphology, and the use of circular aggregates allows the generation and meshing of a statistically large number of numerical specimens with different pore distributions at an acceptable computational cost. Second, previous meso-mechanical studies on cemented backfill have demonstrated that circular or elliptical aggregate simplifications can successfully reproduce the key features of the macroscopic stress-strain response and overall cracking patterns when the matrix-aggregate interface and porosity are properly represented[26]. Third, generating realistic polygonal aggregates would substantially increase model complexity and mesh density, potentially obscuring the specific effects of porosity. Nevertheless, the potential impact of aggregate angularity on local stress concentrations and crack paths is discussed in detail in Section 4.

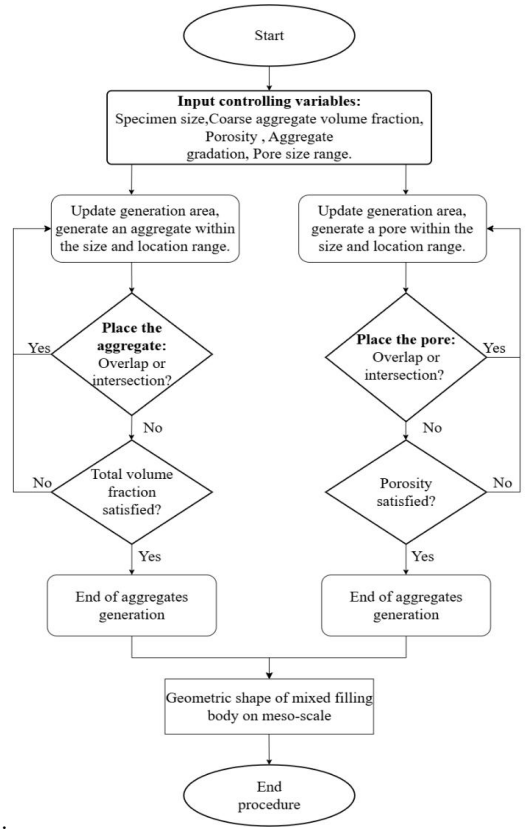

Figure. 1 Algorithm for generation and filling of fine-scale geometries of filling bodies. Prepared and illustrated using Microsoft PowerPoint 2016.

Based on existing studies, researchers have used gray correlation analysis to determine that one important factor affecting the strength of composites is total porosity[34,35]. Therefore, to investigate the effect of different initial defects in the backfill on the specimens, numerical models were developed for porosities of 0%, 0.5%, 1%, and 1.5%. **Figure. 2** shows four numerical models with different porosities. For comparison, three numerical models with the same aggregate and pore distribution and the same porosity were constructed for each case. Uniaxial compression loading simulations were carried out on the four groups of specimens.

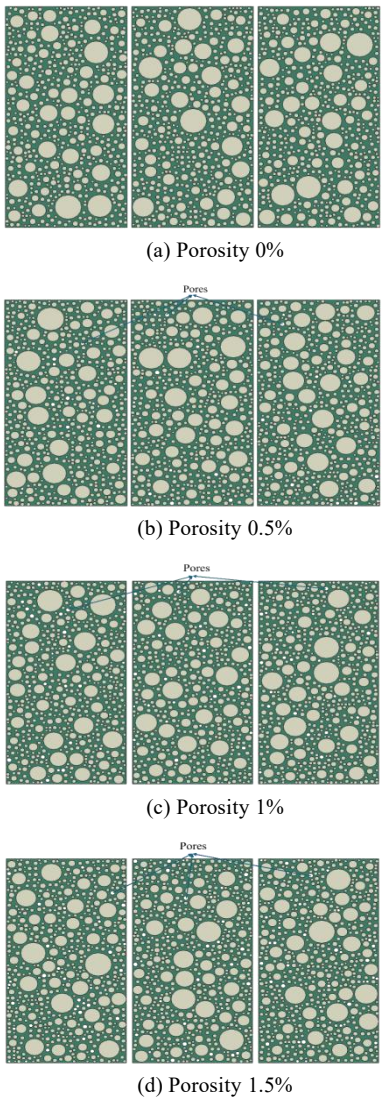

(a) Porosity 0%

(b) Porosity 0.5%

(c) Porosity 1%

(d) Porosity 1.5%

Figure. 2 Meso-scale model of waste tailings consolidated backfill with different porosity. (The filling matrix, waste aggregate and pores are green, grey and white respectively.) (a) Porosity 0%; (b) Porosity 0.5%; (c) Porosity 1%; (d) Porosity 1.5%. The figure was exported from ABAQUS and subsequently edited using Microsoft PowerPoint 2016.

2.3 Mesh Generation and Fracture Modeling

The numerical samples are meshed using the pre-processing function of ABAQUS. Given the known locations of the aggregates and pores, the mortar region is identified through a Boolean operation. The specimens are then meshed using solid finite elements. The mesh size is set in the meshing parameters, and the meshing is performed using the program's automatic meshing method, which allows rapid numerical simulation and statistical analysis of a large number of samples.

The cohesive model can be used as a contact property to simulate crack propagation between two contact surfaces[36]. The cohesive model can be implemented through the use of cohesive elements (viscous elements). The cohesive model determines the extent of damage by applying a fracture criterion. Damage occurs in the cohesive element when the damage criterion is met. At that point, the element begins to degrade according to the predefined damage evolution model. When the element fails completely, the middle layer splits in two, creating geometric discontinuities and thus cracks. This can be described by the traction-separation law[37-39].

To simulate a more realistic fracture process, cohesive interface elements with zero thickness are inserted into the generated solid mesh inside the aggregates. Three sets of cohesive elements with different traction-separation criteria are inserted in the component: cohesive elements inside the aggregate (agg), cohesive elements inside the mortar (mor), and cohesive elements at the aggregate-mortar interface (itz). Given that aggregates have considerably greater strength than cement and ordinary cemented backfill, it is reasonable to conclude that damage is unlikely to occur within the aggregate cohesive elements (agg); likewise, crack formation inside the aggregate is unlikely.

The final finite element mesh after insertion of the cohesive elements (element size = 0.5 mm) is shown in **Figure. 3**. The cohesive elements are highlighted in red. Triangular solid meshes are advantageous because they can adapt effectively to complex geometries, especially curved surfaces and irregular boundaries. The adaptability of triangular meshes facilitates the modeling of realistic and smooth crack paths with greater flexibility.

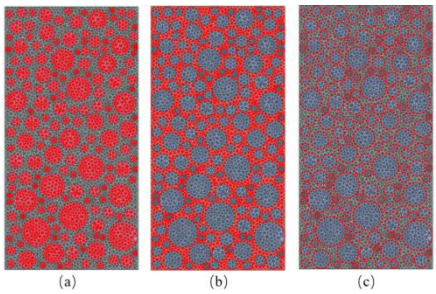

Figure. 3 Finite element meshes with different cohesive force interfaces. (a) in the aggregate, (b) in the mortar and (c) in the aggregate mortar interface. The figure was exported from ABAQUS and subsequently edited using Microsoft PowerPoint 2016.

3.Numerical Simulation and Analysis of Filling Bodies

The material properties are summarized in **Table 2**. The elastic modulus and compressive strength of the mortar matrix were taken from the experimental measurements reported by Chen[40] for cemented backfill with a similar mix proportion (Portland cement binder, waste rock and tailings as aggregate, Talbot gradation index n = 0.6). The tensile strength of the mortar was estimated as approximately 10% of its compressive strength, following the typical ratio for quasi-brittle cementitious materials[30]. The waste rock aggregates were assigned substantially higher stiffness and strength than the mortar[31]. The ITZ was treated as a weakened mortar region with reduced strength and fracture energy, as commonly adopted in meso-scale concrete and backfill models[26,30]. For the cohesive elements, the fracture energies of the mortar and ITZ were estimated from the tensile strength and an assumed characteristic length, and the shear fracture properties were taken to be identical to the normal fracture properties. The solid elements of the waste rock aggregate and mortar were assumed to behave as linear elastic materials.

Table 2. Material properties

	Aggregate	Mortar	CIE-AGG	CIE-MOR	CIE-INT
Young's modulus (MPa)	8,000	2,000	/	/	/
Poisson's ratio	0.23	0.2	/	/	/
Density (10^{-9} tone/mm^3)	2.5	2.3	2.5	2.3	2
Elastic stiffness (MPa/mm)	/	/	8,000	2,000	2,000
Cohesive strength (MPa)	/	/	8	2.5	2
Fracture energy (N/mm)	/	/	0.4	0.1	0.1

In this study, a uniaxial compression test model of a cylindrical numerical specimen with a length of 50 mm and a height of 100 mm was adopted, as shown in **Figure. 4**. All models were completely fixed at the bottom and subjected to uniformly distributed displacement at the top (displacement loading). The lateral boundaries are free (unconstrained) to allow transverse deformation, consistent with standard uniaxial compression test conditions. The simulation adopts the element deletion method: when the element strain exceeds a specified limit, the element is deleted and disappears from the model. During loading, as displacement increases, the number of damaged elements increases, leading to corresponding changes in the number of phase elements. The solid elements of waste aggregate and mortar are assumed to behave as linear elastic. The maximum nominal stress criterion and the linear damage evolution criterion are used[41]. This study shares some of the material properties used in the literature[42]. It is assumed that the shear fracture properties are identical to the normal fracture properties. To investigate the effect of different initial defects, multiple samples of the same type were simulated. Reference samples exhibit a combination of different porosities and identical aggregate content. The simulations are solved using the ABAQUS/Explicit (Dassault Systèmes SIMULIA Corp., Rhode Island, RI, USA) solver, with the analysis step size set to 0.006 s.

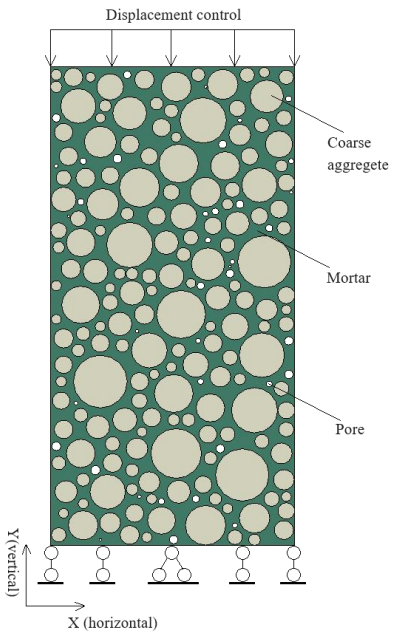

Figure. 4 Boundary conditions and loading mode. Prepared and illustrated using Microsoft PowerPoint 2016.

3.1 Mesh Size Effect

It should be noted that the model is pre-inserted with cohesive elements, which may affect the numerical results. Furthermore, the crack pattern may depend on the mesh because only cohesive elements are capable of cracking. Therefore, a study of the effect of mesh size on model convergence was first performed. Taking a sample with porosity of 0% as an example, the model was meshed with element sizes of 0.500 mm, 0.425 mm, and 0.350 mm. The model with a mesh size of 0.500 mm has 46,404 solid elements and 69,303 cohesive elements, while the numbers for mesh sizes of 0.425 mm and 0.350 mm are 62,379 and 93,212, and 90,664 and 135,566, respectively. From **Figure. 5**, it can be seen that the crack paths are very similar for different mesh sizes in the same frame. Owing to mesh quality, different mesh sizes can produce slightly different crack growth at the aggregate interface. According to the stress data derived from the simulation, the peak stresses for different mesh sizes are 5.36589 MPa, 5.38015 MPa, and 5.53948 MPa, respectively. Overall, the influence of mesh size is minimal. Accordingly, all subsequent numerical simulations use a mesh element size of 0.500 mm.

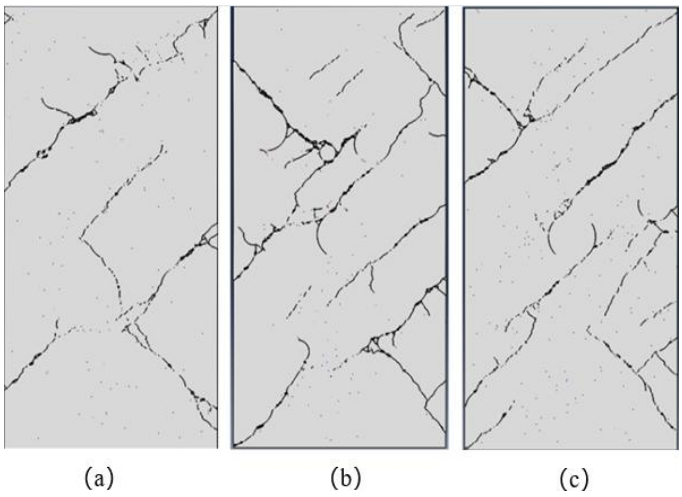

Figure. 5 Crack paths of different mesh sizes. (a) 0.500 mm, (b) 0.425 mm and (c) 0.350 mm. Prepared and illustrated using Microsoft PowerPoint 2016.

3.2 Damage Process and Crack Extension in Filled Body Specimens

The process by which micro-cracks continuously initiate, propagate, and coalesce to form macro-cracks is referred to as damage in the waste rock-tailings cemented body. The cracking characteristics vary significantly depending on the initial defects present. Based on previous research and the model cracking process in this paper[43,44], the damage process of waste rock cemented backfill under uniaxial compression can be divided into four stages: initial pore compaction, linear elastic deformation, yield damage, and post-peak damage. The rupture process of the specimen is described in detail below.

3.2.1 Destruction Process of Non-porous Filler Specimens

With continuous displacement loading, the stress inside the backfill specimen increases and a strip-like stress concentration zone appears. The stress inside the aggregate is greater than that at the edge of the aggregate because of the addition of waste rock aggregate. When loaded for a certain time, the mesh at the edge of the aggregate begins to be damaged and element deletion occurs, forming microcracks around the aggregate edges. With further loading, some microcracks at the aggregate edges propagate, forming multiple cracks that lead to specimen failure. **Figure. 6** illustrates the damage to the component with 0% porosity. Under uniaxial compression, the interface between the coarse aggregate and the cementitious matrix fractures, localized cracks within the backfill accumulate and form macroscopic cracks, and the edges of the specimen dislodge due to the presence of cracks around the specimen. The incorporation of coarse aggregate reinforces fracture slip at the interface between coarse aggregate particles and the cementitious matrix, causing coarse aggregate particles to rub and squeeze against one another. The accumulation of local stresses results in fragmentation of the backfill in the central region, with damage occurring in tension aligned with the loading direction.

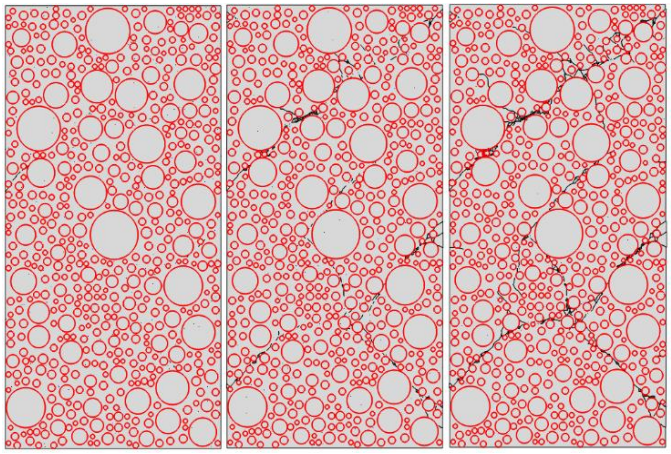

Figure. 6 Destruction process of non-porous specimens. In all panels, the loading direction is vertical (top to bottom). Prepared and illustrated using Microsoft PowerPoint 2016.

3.2.2 Destruction Process of Specimens with Pore-filled Bodies

The damage process of porous backfill specimens is analogous to that of non-porous specimens, but the presence of pores imparts distinctive characteristics. **Figure. 7** shows the failure process for specimens with porosities of 0.5%, 1%, and 1.5%, respectively. At the initial stage of loading, most microcracks are generated at the edges of the pores, with the majority of damage concentrated in pore-rich regions around the specimen. This occurs because the stress concentration in these regions is more intense, and some cracks also form around the aggregate in areas closer to the pores. As loading continues, the pore structure undergoes transformation, accompanied by an increase in the number and extent of microcracks. Damage propagates from the periphery to the center of the specimen, suggesting that pores facilitate damage expansion. As microcracks around multiple pores expand, pore-to-pore, pore-to-aggregate, and aggregate-to-aggregate penetration cracks form, fracture surfaces develop, and damage to the backfill progresses in an orderly manner from local to global.

As illustrated in the figure, pores result in more pronounced localization of damage in the cement mortar. Despite the presence of pores, the aggregate-mortar interface exhibits the greatest degree of deterioration. The pore structure significantly influences the location of macro-crack initiation and the direction of propagation. Consequently, macro-cracks must traverse the pore-aggregate-mortar interface. It can thus be concluded that the structure of the backfill, the number of pores, and the water-to-cement (w/c) ratio all significantly affect the performance of the backfill. The cement strength is lower than the strength of the waste rock, and specimen damage is mainly caused by insufficient cement strength. Cracks eventually lead to specimen failure. Cracks are generated at pores as well as at the edges of aggregate particles.

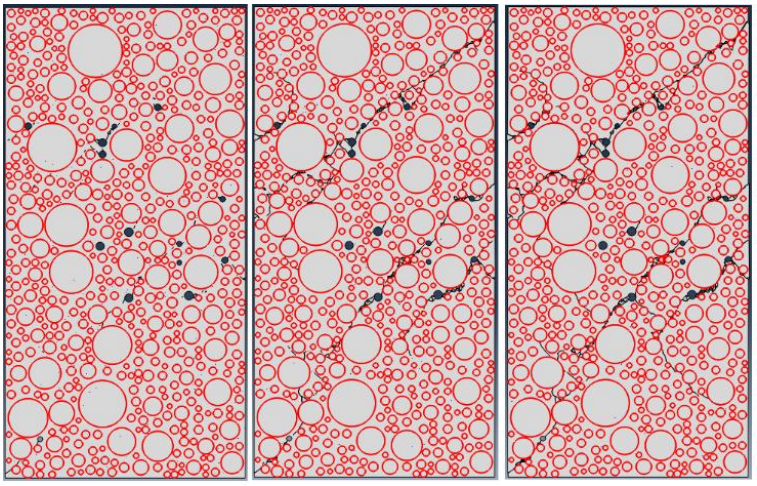

(a) Porosity 0.5%

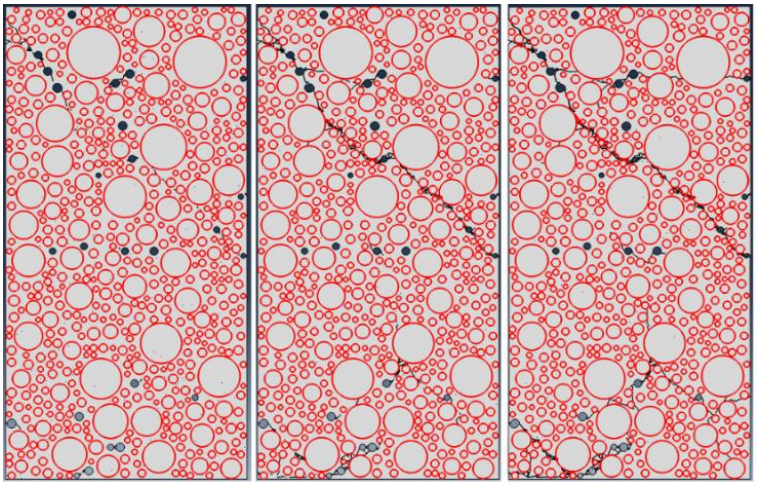

(b) Porosity 0.5%

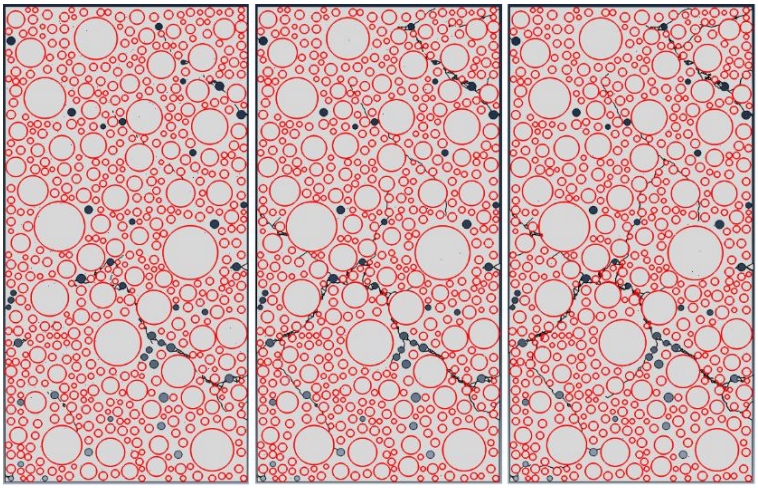

(c) Porosity 0.5%

Figure. 7 Destruction process of specimens with different porosities. In all panels, the loading direction is vertical (top to bottom). (a) Porosity is 0.5%; (b) Porosity is 1%; (c) Porosity is 1.5%. Prepared and illustrated using Microsoft PowerPoint 2016.

3.3 Characterization of Cracks in the Filling Body

3.3.1 Number of Rupture Units of Filled Body Specimens

Figure. 8 shows the evolution of the number of ruptured elements during uniaxial compression for specimens with different porosities. Across all specimens, no ruptured elements appear before an analysis step time of 0.002 s, indicating no crack initiation. Between 0.002 s and 0.003 s, the number of ruptured elements increases sharply and subsequently stabilizes, marking the period during which microcracks initiate, propagate, and coalesce into macroscopic failure.

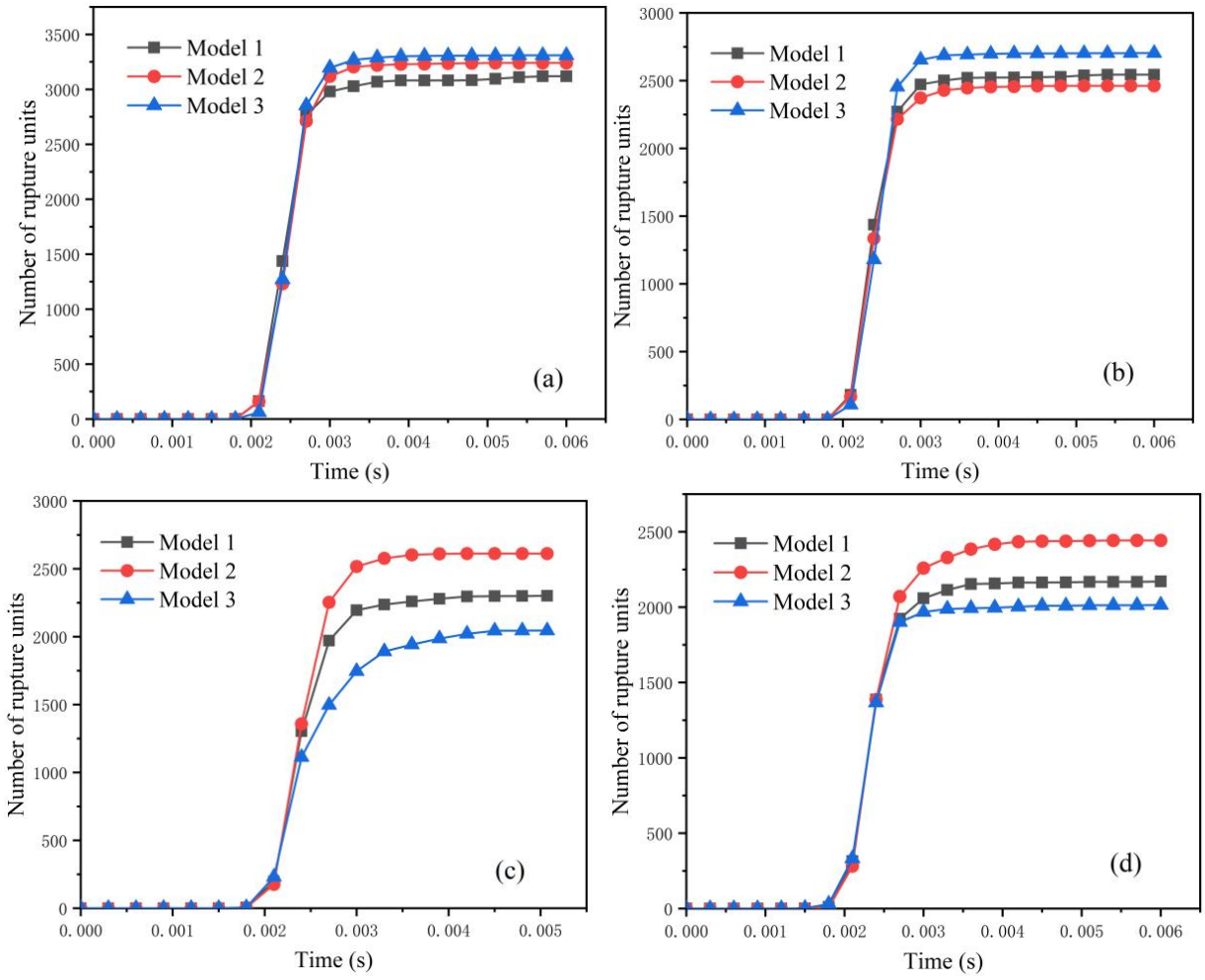

Figure. 8 Number of rupture units of the filled body specimen during compression. (a) porosity is 0%; (b) porosity is 0.5%; (c) porosity is 1%; (d) porosity is 1.5%. Prepared and illustrated using Origin 2018.

Table 3 summarizes the ruptured element counts for specimens with different porosities. For specimens with 0% porosity, the total numbers of ruptured elements are 3,120, 3,241, and 3,310, giving an average of 3,324. The corresponding average values for porosities of 0.5%, 1%, and 1.5% are 2,570, 2,322, and 2,210, respectively. As porosity increases, the number of ruptured elements under uniaxial compression decreases. This indicates that specimens with higher porosity develop fewer cracks, which may be because pores act as the primary sites for crack initiation. Once the microcracks around pores coalesce into macroscopic damage, the crack network stabilizes and further rupture events become limited. Comparison of the damage processes of specimens with different porosities (**Figure. 7**) shows that microcracks tend to emerge near pores during the initial loading phase. The presence of pores reduces the local strength around pores, so the probability of cracks forming around pores is higher than around aggregates. Furthermore, the 0% porosity specimen exhibits a greater average number of ruptured elements than the porous specimens. This is because, in the absence of pores, microcracks form around aggregates, and the internal strength is more uniform, reducing the likelihood of internal cracking. Subsequently, as cracks advance to a certain degree, specimens with or without pores are essentially analyzed concurrently at the same time, evidenced by a sharp increase in ruptured elements, reaching a maximum and then stabilizing. This indicates that crack expansion has ceased and the specimen has reached its maximum strength and undergone complete failure. The comparative analysis in **Figure. 8** demonstrates that the number of ruptured elements of the 0% porosity specimen reaches its maximum value slightly later than that of the porous specimens. This further indicates that the number of ruptured elements in 0% porosity specimens is larger than in specimens with 0.5%, 1%, and 1.5% porosity.

Table 3. Number of rupture units in filled body specimens with different porosities

	Model 1	Model 2	Model 3
Porosity 0%	3,120	3,241	3,310
Porosity 0.5%	2,544	2,462	2,703
Porosity 1%	2,301	2,613	2,051
Porosity 1.5%	2,171	2,443	2,015

3.3.2 Crack Length of Filled Body Specimen

Figure. 9 presents the evolution of total crack length during uniaxial compression. Consistent with the ruptured element data, crack length remains zero before 0.002 s, increases sharply between 0.002 s and 0.003 s, and then plateaus, confirming that crack initiation and propagation are concentrated within this narrow time window.

The crack length data for specimens with different porosities were analyzed. The crack lengths for 0% porosity specimens are

158.54 mm, 163.24 mm, and 167.34 mm, with an average of 163.04 mm. The average crack lengths for 0.5%, 1%, and 1.5% porosity are 135.91 mm, 116.88 mm, and 110.98 mm, respectively. Thus, as porosity increases, the crack length under uniaxial compression decreases continuously, consistent with the trend in the number of ruptured elements. The increase in porosity leads to earlier damage of the specimens, as seen in **Figure. 9**, where the slope of the curve increases with porosity between analysis step times of 0.0015 and 0.0020 s. This again indicates that higher porosity results in earlier crack initiation and damage.

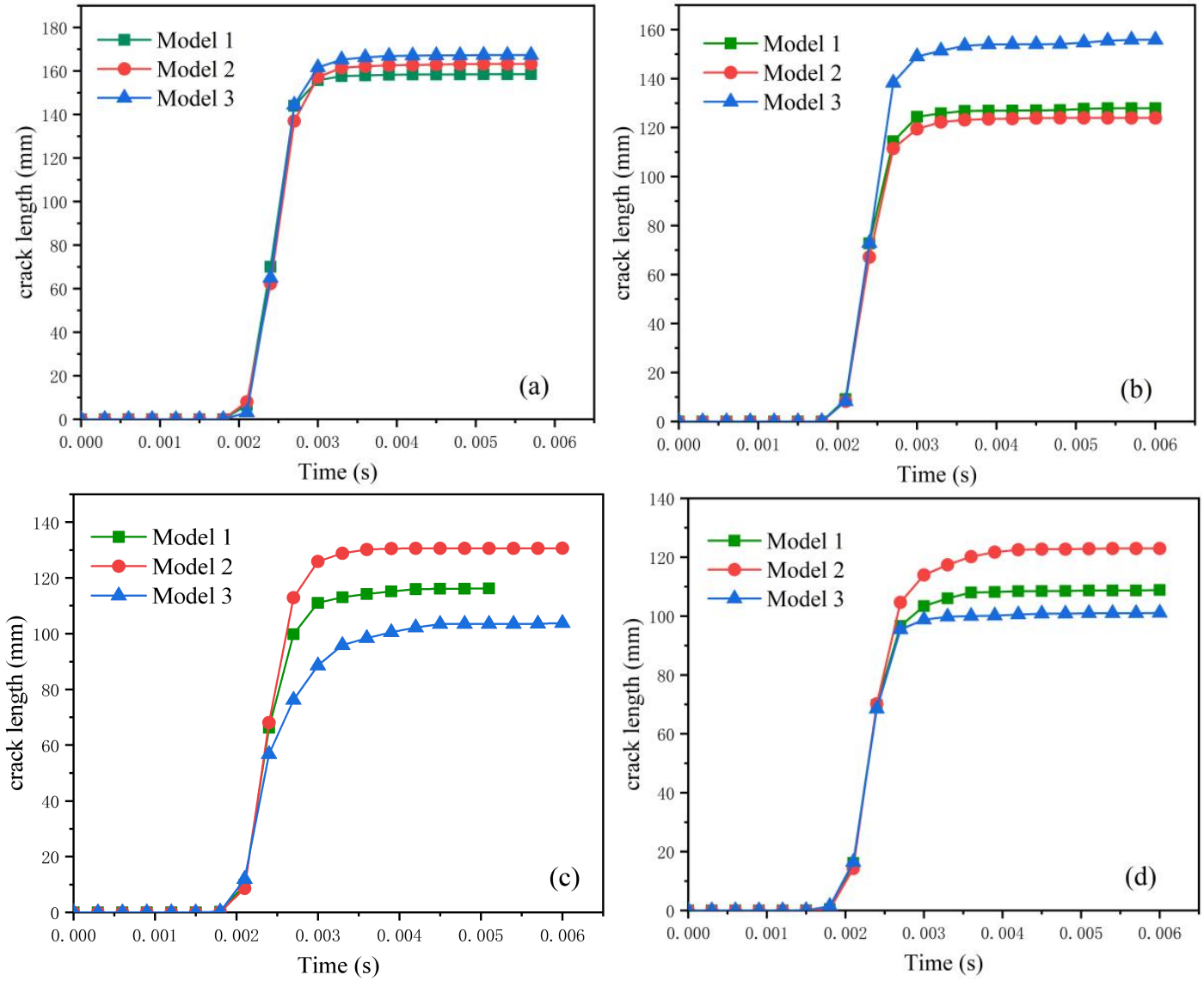

Figure. 9 Crack length of the filled body specimen. (a) porosity is 0%; (b) porosity is 0.5%; (c) porosity is 1%; (d) porosity is 1.5%. Prepared and illustrated using Origin 2018.

3.4 Stress-strain Curve

Figure. 10 illustrates the stress-strain curves of backfill specimens under varying porosity. From analysis of the curves, the deformation and damage of waste rock-tailings cemented backfill under uniaxial compression can be broadly classified into four stages, as outlined below:

(1) Initial pore compaction stage. In this phase, the initial pores within the backfill are progressively compacted, resulting in an upward-convex shape of the stress-strain curve. Because the backfill is a composite of waste rock and tailings sand as the filling aggregate, its particle size is considerable, making the presence of primary pores inevitable. Consequently, the compaction process is more pronounced in the overall failure process.

(2) Linear elastic deformation stage. In this phase, the axial stress increases approximately linearly with strain. When the stress reaches the initial cracking stress (typically 75% of the peak stress), the backfill specimen is on the verge of entering the yield damage stage.

(3) Yield damage stage. At this juncture, the growth rate of axial stress begins to decelerate, and the stress-strain curve exhibits a concave shape. When the stress reaches its maximum at a specific point, that value is referred to as the peak stress. Once the stress exceeds the peak stress, the backfill transitions into the post-peak damage stage.

(4) Post-peak damage stage. In this stage, the stress decreases sharply with increasing strain, and the backfill specimen develops penetrating cracks (macroscopic damage cracks). When the stress reaches a certain value, the backfill undergoes complete failure, but owing to residual stress, it still retains some bearing capacity after failure.

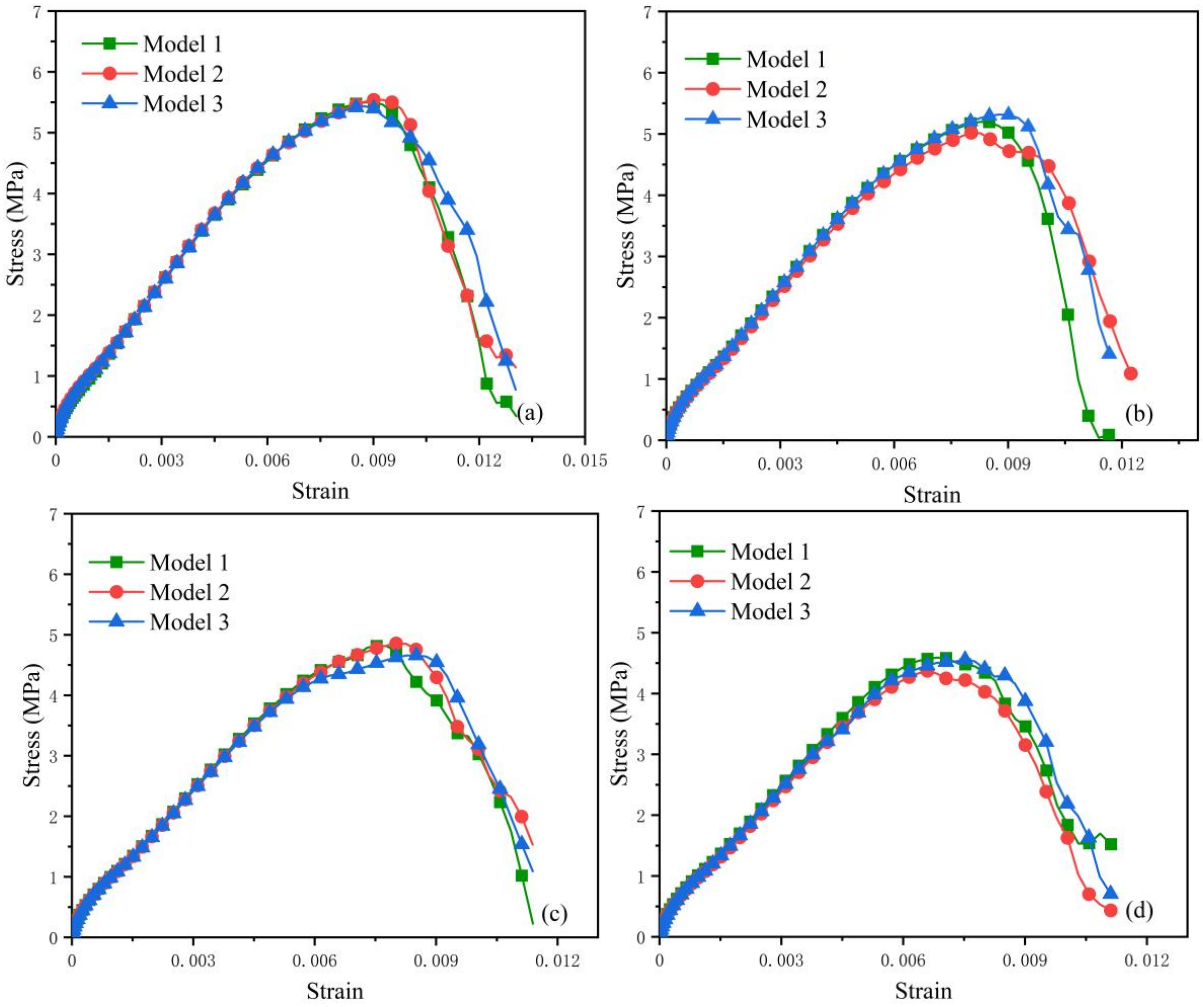

Figure. 10 Stress-strain curves of specimens with different porosity values. (a) the porosity is 0%; (b) A porosity of 0.5 %; (c) A porosity of 1%; (d) The porosity is 1.5 %. Prepared and illustrated using Origin 2018.

Peak stress and peak strain (the axial strain corresponding to peak stress) are the main parameters for studying the mechanical properties of cemented materials. The stress-strain data show that under the same porosity, the curves of Model 1, Model 2, and Model 3 differ slightly because of the random distribution of aggregates and different internal structures. For the 0% porosity specimen, the three models exhibit an average peak stress of approximately 5.37 MPa, with a range (maximum minus minimum) of 0.104 MPa, i.e., a variation of 1.8% about the mean. The peak stress ranges for 0.5%, 1%, and 1.5% porosity are 0.298 MPa, 0.199 MPa, and 0.183 MPa, respectively, corresponding to reductions of 5.6%, 4.1%, and 4%. Many reasons can contribute to these variations, such as the influence of aggregate distribution. Due to space limitations, this paper focuses only on different initial defects in backfill specimens. In summary, as porosity increases, the strength of the specimen continuously decreases, and the peak stress of the numerical specimens shows a downward trend. Increased porosity in the backfill leads to loosening of the internal structure, thus reducing its deformation resistance. As the initial defect increases, both peak stress and peak strain gradually decrease, and the mechanical properties gradually deteriorate.

In this paper, the numerical simulation results of the backfill are compared with the experimental results from the literature[42]. Under comparable grading indices, the numerical specimens exhibited final failure patterns similar to those observed experimentally, with both shear and tensile damage modes present, regardless of whether pores were explicitly modeled. In the experiments, as the grading index increased, the dominant failure mode gradually transitioned from shear to tensile damage; in the numerical models, the proportions of these two modes may differ somewhat owing to the simplified circular aggregate geometry and assumed material homogeneity. **Figure. 11** presents a comparison of the stress-strain curves. Quantitative validation between the numerical simulations and experimental data reported by Chen[42] reveals that the simulated average peak strength is 5.37 MPa, versus an experimental value of 5.21 MPa, yielding a relative error of 3.07%. The peak strain is 0.0120 in the simulation compared with 0.0115 in the experiment (relative error of 4.35%). These relative errors are all within 5%, confirming that the meso-scale mechanical parameters adopted in the simulation yield responses that are generally consistent with the experimental measurements and that the peak stresses are in close agreement. This comparison validates the two-dimensional meso-scale modeling strategy employed in this study. This study offers novel insights into predicting the macroscopic mechanical properties of waste rock-tailings cemented backfill containing diverse initial defects. Furthermore, the proposed simulation method can be integrated with experimental design strategies to facilitate the selection of optimal levels for key influencing factors, thereby improving the overall backfill performance. It also has a certain guiding role in backfill structure design.

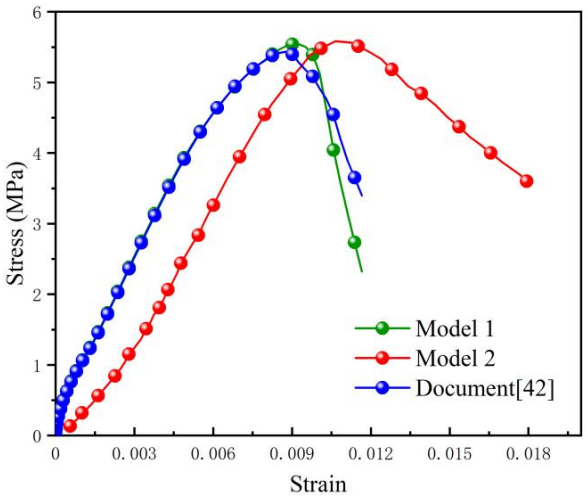

Figure. 11 Comparison of uniaxial compression stress-strain curves. Prepared and illustrated using Origin 2018.

Although the absolute values and detailed crack morphologies might be affected by aggregate angularity, the combined analysis of crack patterns, ruptured element statistics, and stress-strain behavior. In non-porous specimens, cracks initiate predominantly at the aggregate-mortar interface, where the elastic mismatch between stiff aggregate and soft mortar creates stress concentrations. In porous specimens, however, pores introduce free surfaces with near-zero local stiffness, generating stress concentrations that exceed those at the aggregate-mortar interface. Consequently, cracks nucleate preferentially at pore boundaries. This explains the shift in crack initiation sites observed in **Figure. 6** and **Figure. 7**. As porosity increases, individual pores act as stress concentrators that localize damage in their immediate vicinity. Microcracks initiate early at pore edges, and because stress is relieved once these local cracks coalesce, fewer additional cracks form elsewhere in the specimen. This localization effect explains why higher porosity leads to fewer ruptured cohesive elements and shorter total crack length (**Figure. 8** and **Figure. 9**), even though damage initiates earlier. The 18.6% reduction in compressive strength when porosity increases from 0% to 1.5% (**Figure. 10**) is attributed to two factors. First, pores reduce the effective load-bearing cross-sectional area. Second, and more importantly, early crack initiation at pore boundaries reduces the stress level at which the specimen transitions from distributed microcracking to localized macro-fracture, thereby lowering the peak stress. Despite this reduction, the fundamental four-stage failure sequence (compaction, elastic deformation, yielding, post-peak softening) remains unchanged because the failure mode is governed by the tensile strength of the mortar and ITZ, which are unaffected by porosity. Regarding the influence of pore size and distribution, the present models assume circular pores of uniform size (1 mm – 2 mm). In real backfill, pore sizes and spatial distributions are heterogeneous. Larger or clustered pores would be expected to intensify local stress concentration and further reduce strength, while more uniformly distributed fine pores may have a less pronounced effect. A systematic investigation of pore size polydispersity and spatial distribution patterns is warranted in future work. It should be noted that this mechanistic interpretation is based on circular aggregate simplification; the potential influence of aggregate angularity on stress concentrations and crack paths is discussed in Section 4. Semi-quantitatively, based on meso-scale studies of concrete and cemented backfill[26,32], angular aggregates can induce 10% – 30% higher local stress concentrations at the aggregate-mortar interface compared with circular aggregates, potentially leading to a 5% – 10% overestimation of uniaxial compressive strength in the present circular-aggregate models. However, the key finding that porosity increases from 0% to 1.5% reduces strength by 18.6% reflects a relative trend that is expected to remain valid regardless of aggregate shape, because porosity dominates the fracture mechanism under uniaxial compression.

4.Limitations and Future Prospects

In this study, aggregates were simplified as circles, which facilitates model generation and convergence while isolating the effect of porosity. However, in real cemented waste rock backfill, the crushed waste rock particles typically possess angular edges and sharp corners. Such angular aggregates can generate higher local stress concentrations around the interfacial transition zone, potentially initiating interfacial debonding at lower global stress levels and altering crack propagation trajectories. Compared with circular aggregates, angular particles may lead to more tortuous crack paths, an increased tendency for crack branching, and possibly a reduction in uniaxial compressive strength for the same aggregate volume and porosity. The present models may therefore, to some extent, underestimate the heterogeneity of the stress field and the complexity of the fracture network. Despite these limitations, the circular aggregate idealization adopted here serves as a well-controlled benchmark for revealing the dominant role of porosity in meso-scale fracture evolution. The qualitative trends observed in crack number, crack length, and strength reduction with increasing porosity are expected to remain valid, although the absolute values and detailed crack morphologies might be affected by aggregate angularity.

Additionally, in the present cohesive zone model, the shear fracture properties of the mortar and ITZ were assumed to be identical to the normal fracture properties (both 0.1 N/mm). For quasi-brittle cemented backfill materials, the shear fracture energy is typically larger than the tensile fracture energy due to frictional dissipation and aggregate interlocking. This simplification may therefore underestimate the actual fracture resistance under shear-dominant conditions. However, because uniaxial compression loading primarily induces tensile splitting failure, the influence of this assumption on the reported compressive strength and porosity-related trends is expected to be minor. Future work should incorporate separate shear and normal fracture energies calibrated from mixed-mode fracture tests.

Future work should incorporate realistic aggregate shapes, such as random convex polygons generated from actual particle image analysis and systematically compare the failure mechanisms between circular and angular aggregate models under identical porosity conditions. Furthermore, the intrinsic heterogeneity of the backfill matrix and the ITZ, as well as true triaxial or dynamic loading conditions relevant to underground stopes, should be integrated to construct more comprehensive and predictive numerical frameworks.

5. Conclusions

In this study, the backfill was modeled as comprising the backfill matrix, waste aggregate, pores, and the interface between the aggregate and the matrix. The initiation and propagation of complex mesoscale cracks were simulated using the preinserted cohesive interface element technique. Based on a two-dimensional micromodel with porosities ranging from 0% to 1.5%, the effects of porosity on the uniaxial compression properties of the backfill were systematically discussed in terms of crack initiation and propagation

mechanisms, crack characteristics, and stress-strain relationships. The following conclusions were drawn from the two-dimensional microscopic simulation:

(1) The damage processes of the models with and without porosity are analogous; the damage mode is tensile and is aligned with the loading direction. In the non-porous model, cracks emerge at the edges of aggregates and propagate; in the porous model, the majority of cracks originate at the edges of pores and then extend. The presence of pores significantly impacts the initiation and propagation of macro-cracks, as cracks must traverse the pore-aggregate-slurry interface.

(2) With increasing porosity, both the number of ruptured elements and the total crack length decrease monotonically. Analysis of the evolution curves shows that damage initiates earlier in specimens with higher porosity. This is because pores act as preferential crack nucleation sites, and the early localization of damage around pores limits the development of a distributed crack network elsewhere in the specimen.

(3) As porosity increased from 0% to 1.5%, the uniaxial compressive strength decreased by 18.6%. This strength reduction arises from the combined effect of reduced load-bearing area and early crack initiation at pore boundaries, which lowers the stress threshold for the transition to macroscopic fracture. However, the fundamental four-stage failure sequence remains unchanged because it is governed by the intrinsic tensile strength of the mortar and ITZ phases.

Author Contributions

Kang Zhao: Methodology; Supervision; Daotan Wen: Conceptualization; Writing- Reviewing and Editing; Writing-Original draft preparation; Weiling Xiao: Investigation; Validation; Yajing Yan: Visualization, Investigation; Validation; Juncheng Zhong: Data curation; Software.

Data Availability

The data supporting the findings of this study are available from the corresponding author upon reasonable request.

Funding

The study has been supported by the National Natural Science Foundation (Grant No. 52374138, 52574163).

Conflicts of Interest

No conflict of interest exists in the submission of this manuscript, and the manuscript is approved by all authors for publication. I declare on behalf of my co-authors that the work described is original research that has not been published previously and is not under consideration for publication elsewhere, in whole or in part. All the listed authors have approved the enclosed manuscript.

Reference

[1] Zhang S, Shi T, Ni W, *et al*. The mechanism of hydrating and solidifying green mine fill materials using circulating fluidized bed fly ash-slag-based agent. *J Hazard Mater*. 2021, 415. [Google Scholar] [CrossRef]

[2] Peng, L.I, Mei-feng C.A.I. Challenges and new insights for exploitation of deep underground metal mineral resources. *Transactions of Nonferrous Metals Society of China*. 2021, 31 (11): 3478-3505. [Google Scholar] [CrossRef]

[3] Wang S F, Sun L, Huang L, *et al*. Non-explosive mining and waste utilization for achieving green mining in underground hard rock mine in China. *Transactions of Nonferrous Metals Society of China*. 2019, 29 (9): 1914-1928. [Google Scholar] [CrossRef]

[4] Farjana S H, Huda N, Mahmud M A P, *et al*. A Review on Impact of Mining and Mineral Processing Industries through Life Cycle Assessment. *Journal of Cleaner Production*. 2019, 231: 1200-1217. [Google Scholar] [CrossRef]

[5] Marzoughi, O, Pickles, C.A. 2024. Solid state reduction and magnetic separation of nickeliferous laterite ores: Review and analysis. *Journal of Industrial and Engineering Chemistry*. 2024, 140: 65-87. [Google Scholar] [CrossRef]

[6] Zhao Y, Zhao G, Zhou J, *et al*. Mining Stress Evolution Law of Inclined Backfilled Stopes Considering the Brittle-Ductile Transition in Deep Mining. *Mathematics*. 2022, 10 (8): 1308. [Google Scholar] [CrossRef]

[7] Fall M, Célestin J C, Pokharel M, *et al*. A contribution to understanding the effects of curing temperature on the mechanical properties of mine cemented tailings backfill. *Engineering Geology*. 2010, 114 (3-4): 397-413. [Google Scholar] [CrossRef]

[8] Xue G, Yilmaz E, Song W, *et al*. Mechanical, flexural and microstructural properties of cement-tailings matrix composites: Effects of fiber type and dosage. *Composites Part B: Engineering*. 2019, 172: 131-142. [Google Scholar] [CrossRef]

[9] Chen S, Du Z, Zhang Z, *et al*. Effects of chloride on the early mechanical properties and microstructure of gangue-cemented paste backfill. *Construction and Building Materials*. 2020, 235. [Google Scholar] [CrossRef]

[10] Wang Y, Lu H, Wu J. Experimental investigation on strength and failure characteristics of cemented paste backfill-rock composite under uniaxial compression. *Construction and Building Materials*. 2021, 304. [Google Scholar] [CrossRef]

[11] Zhao K, Lai Y, He Z, *et al*. Study on energy dissipation and acoustic emission characteristics of fiber tailings cemented backfill with different ash-sand ratios. *Process Safety and Environmental Protection*. 2023, 174: 983-996. [Google Scholar] [CrossRef]

[12] Gao R, Wang W, Xiong X, *et al*. Effect of curing temperature on the mechanical properties and pore structure of cemented backfill materials with waste rock-tailings. *Construction and Building Materials*. 2023, 409. [Google Scholar] [CrossRef]

[13] Gao T, Wu A, Wang S, *et al*. Experimental and numerical investigations of bending mechanical properties and fracture characteristics of cemented tailings-waste rock backfill under three-point bending. *Construction and Building Materials*. 2024, 447. [Google Scholar] [CrossRef]

[14] Yan B, Jia H, Yilmaz E, *et al*. Numerical study on microscale and macroscale strength behaviors of hardening cemented paste backfill. *Construction and Building Materials*. 2022, 321. [Google Scholar] [CrossRef]

[15] Yang T, Wang J, Qiao D, *et al*. The thixotropic characteristics of rheological parameters of waste stone-tailings cemented paste backfill and the time effect of pipeline resistance. *Construction and Building Materials*. 2024, 423. [Google Scholar] [CrossRef]

[16] Zhu T, Chen Z, Cao J, *et al*. Investigation of the fracture behavior of cemented waste rock-tailing backfill by digital image correlation technique and discrete element modeling. *Construction and Building*

Materials. 2024, 428. [Google Scholar] [CrossRef]

[17] Jiao H, Zhang W, Yang Y, *et al*. Static mechanical characteristics and meso-damage evolution characteristics of layered backfill under the condition of inclined interface. *Construction and Building Materials*. 2023, 366. [Google Scholar] [CrossRef]

[18] Yuan G, Zhang J, Ren Z, *et al*. Research on mechanical performance and micro-structural characteristics for large graded aggregates. *Construction and Building Materials*. 2022, 341. [Google Scholar] [CrossRef]

[19] Zhou Y, Yan Y, Zhao K, *et al*. Study of the effect of loading modes on the acoustic emission fractal and damage characteristics of cemented paste backfill. *Construction and Building Materials*. 2021, 277. [Google Scholar] [CrossRef]

[20] Gao Z, Wu D, Wu H, *et al*. Numerical Simulation Study on the Influence of Fracture on Borehole Wave Modes: Insights from Fracture Width, Filling Condition, and Acoustic Frequency. *Sensors*. 2024, 24 (12): 3955. [Google Scholar] [CrossRef]

[21] Wang Z, Chen M, Liao Y. Analysis of Fire Resistance of Prestressed Concrete T-Beam Based on ABAQUS Numerical Simulation. *Applied Sciences*. 2023, 13 (8): 4683. [Google Scholar] [CrossRef]

[22] Zhang J, Liu Z, Ong M C, *et al*. Numerical simulations of the sliding impact between an ice floe and a ship hull structure in ABAQUS. *Engineering Structures*. 2022, 273. [Google Scholar] [CrossRef]

[23] Tullu A, Ku T W, Kang B S. Elastic deformation of fiber-reinforced multi-layered composite conical shell of variable stiffness. *Composite Structures*. 2016, 154: 634-645. [Google Scholar] [CrossRef]

[24] Huang D, Wang X, Chang X, *et al*. Evolution law study of pore and fracture of coal gangue cemented filling body under axial compression using PFC2D. *Construction and Building Materials*. 2024, 411. [Google Scholar] [CrossRef]

[25] Xu Y, Zhao S, Jin G, *et al*. Explicit dynamic fracture simulation of two-phase materials using a novel meso-structure modelling approach. *Composite Structures*. 2019, 208: 407-417. [Google Scholar] [CrossRef]

[26] Xin L. Meso-scale modeling of the influence of waste rock content on mechanical behavior of cemented tailings backfill. *Construction and Building Materials*. 2021, 307. [Google Scholar] [CrossRef]

[27] Wang H, Feng G, Qi T, *et al*. Insight into the fracture mechanical properties of the interfacial transition zone of cemented coal gangue backfill under different stress angles by mesoscopic digital image correlation. *Engineering Fracture Mechanics*. 2024, 300. [Google Scholar] [CrossRef]

[28] Shi X, Feng G, Bai J, *et al*. Brazil splitting characteristics of coal-backfilling composite structure with different interface angles: Insights from laboratory experiment and numerical simulation. *Journal of Central South University*. 2023, 30 (1): 189-201. [Google Scholar] [CrossRef]

[29] Zhao K, Ma C, Yang J, *et al*. Pore fractal characteristics of fiber-reinforced backfill based on nuclear magnetic resonance. *Powder Technology*. 2023, 426. [Google Scholar] [CrossRef]

[30] Kim S M, Al-Rub R K A. Meso-scale computational modeling of the plastic-damage response of cementitious composites. *Cement and Concrete Research*. 2011, 41 (3): 339-358. [Google Scholar] [CrossRef]

[31] Chen G, Yao N, Ye Y, *et al*. Study on mechanical properties and damage characteristics of cemented waste rock-tailing backfill. *Environmental Science and Pollution Research*. 2023, 30 (46): 102181-102197. [Google Scholar] [CrossRef]

[32] Rao W, Zhang J, Jiang H, *et al*. Meso-mechanical constitutive model of bulk metallic glass matrix composites. *Mechanics of Materials*. 2016, 103: 68-77. [Google Scholar] [CrossRef]

[33] Zhang W, Zhou Z, Scarpa F, *et al*. A fatigue damage meso-model for fiber-reinforced composites with stress ratio effect. *Materials & Design*. 2016, 107: 212-220. [Google Scholar] [CrossRef]

[34] Park J M, Lee B C, Chae S W, *et al*. Surface reconstruction from FE mesh model. *Journal of Computational Design and Engineering*. 2019, 6 (2): 197-208. [Google Scholar] [CrossRef]

[35] Song W, Zhang M, Wu H. Gray correlation analysis between mechanical performance and pore characteristics of permeable concrete. *Journal of Building Engineering*. 2024, 86. [Google Scholar] [CrossRef]

[36] Zhou M, Dong W. Grey correlation analysis of macro- and micro-scale properties of aeolian sand concrete under the salt freezing effect. *Structures*. 2023, 58. [Google Scholar] [CrossRef]

[37] Linke M, Lammering R. On the calibration of the cohesive strength for cohesive zone models in finite element analyses. *Theoretical and Applied Fracture Mechanics*. 2023, 124. [Google Scholar] [CrossRef]

[38] Carol I, López C M, Roa O. Micromechanical analysis of quasi-brittle materials using fracture-based interface elements. *International Journal for Numerical Methods in Engineering*. 2001, 52 (1-2): 193-215. [Google Scholar] [CrossRef]

[39] López C M, Carol I, Aguado A. 2007. Meso-structural study of concrete fracture using interface elements. I: numerical model and tensile behavior. *Materials and Structures*. 2008, 41 (3): 583-599. [Google Scholar] [CrossRef]

[40] Yang Z J, Su X T, Chen J F, *et al*. Monte Carlo simulation of complex cohesive fracture in random heterogeneous quasi-brittle materials. *International Journal of Solids and Structures*. 2009, 46 (17): 3222-3234. [Google Scholar] [CrossRef]

[41] Brünig M, Gerke S, Hagenbrock V. Stress-state-dependence of damage strain rate tensors caused by growth and coalescence of micro-defects. *International Journal of Plasticity*. 2014, 63: 49-63. [Google Scholar] [CrossRef]

[42] Chen G, Ye Y, Yao N, *et al*. Deformation failure and acoustic emission characteristics of continuous graded waste rock cemented backfill under uniaxial compression. *Environmental Science and Pollution Research*. 2022, 29 (53): 80109-80122. [Google Scholar] [CrossRef]

[43] Chen G, Ye Y, Yao N, *et al*. Experimental study on mechanical strength and acoustic emission characteristics of waste rock cemented backfill. *Bulletin of Engineering Geology and the Environment*. 2024, 83 (4): 133. [Google Scholar] [CrossRef]

[44] Zhang J, Yang K, He X, *et al*. Study on mechanical properties and damage characteristics of coal-based solid waste cemented backfill. *Construction and Building Materials*. 2023, 368. [Google Scholar] [CrossRef]